

Supplementary information

Sustainable N-doped lignin-derived porous carbon showing ion selectivity in capacitive deionization applications

Saowaluk Chaleawlert-umpon*, Supaporn Phiromrak, Nuttaporn Pimpha

National Nanotechnology Center, National Science and Technology Development Agency,
Thailand Science Park, Pathum Thani 12120, Thailand

*E-mail: saowaluk@nanotec.or.th

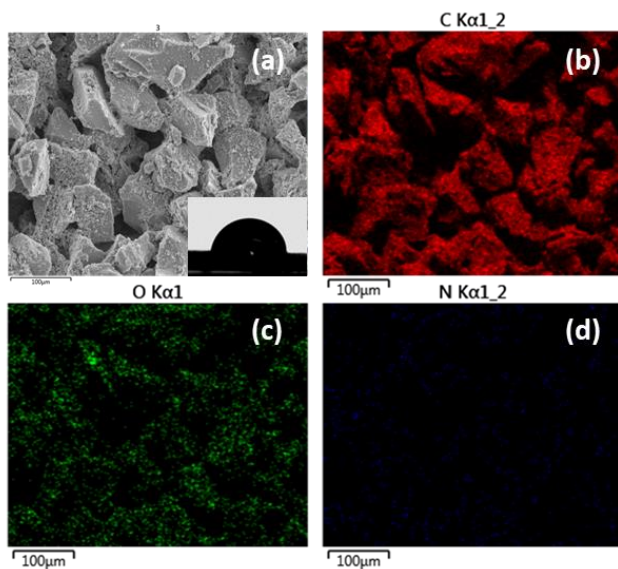


Fig. S1 SEM image (a) with an insert showing a photo of water contact angle; and SEM-EDX mapping with C (b), O (c), and N (d) of the LC electrode.

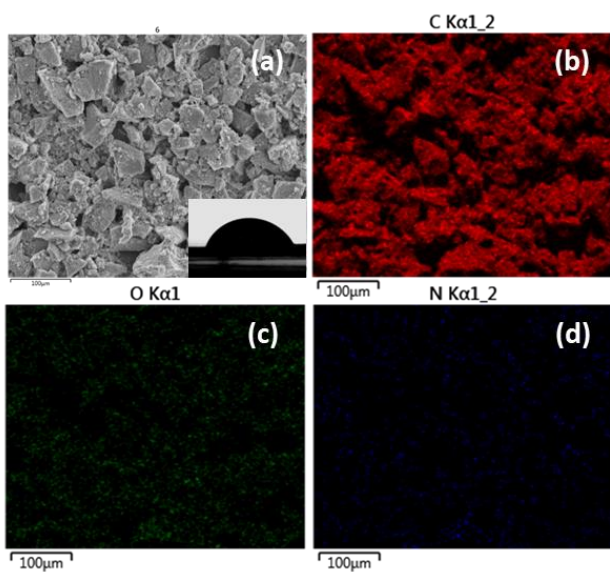


Fig. S2 SEM image (a) with an insert showing a photo of water contact angle; and SEM-EDX mapping with C (b), O (c), and N (d) of the NLC electrode.

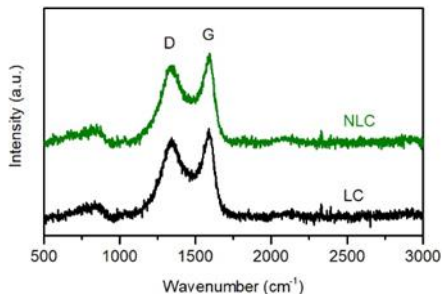


Fig. S3 Raman spectra of LC and NLC.

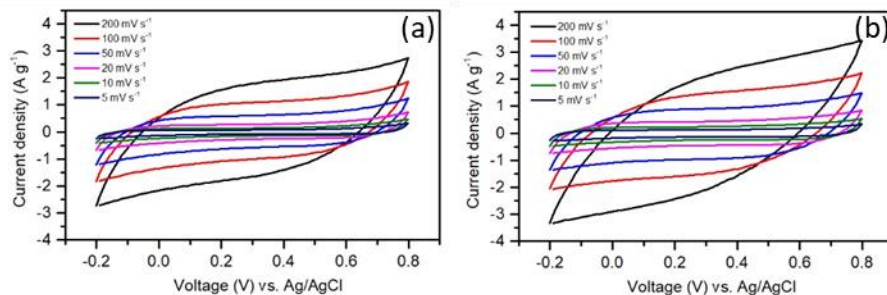


Fig. S4 CV curves of the LC (a) and NLC (b) electrodes with various scan rates measured in 0.5 M NaCl solution.

Fig. S4 presents the CV curves as a function of scan rate of the LC and NLC electrodes in 0.5 M NaCl solution. All showed a rectangular shape with a slight deviation in a high scan rate (100-200 mV s^{-1}). The CV curves of the NLC electrodes had a larger area than those of the LC electrodes.

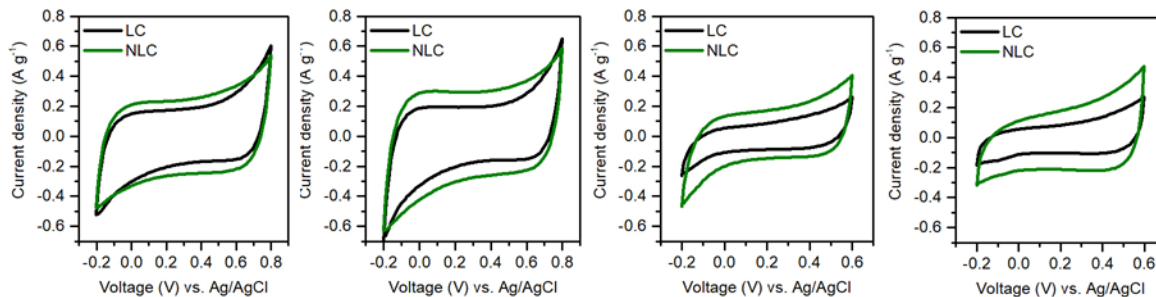


Fig. S5 CV curves of the LC and NLC electrodes in 0.5 M NaCl (a), KCl (b), MgCl_2 (c), CaCl_2 (d) at a scan rate of 10 mV s^{-1} .

Fig. S5 exhibits the CV profiles of the LC and NLC electrodes in different salt solutions. All curves were relatively rectangular shape without redox peaks appearing in the chosen potential range, indicating the capacitive behavior. The specific capacitances of the NLC electrode were higher than those of the LC electrode in all salt solutions. It was corresponded with their individual specific surface areas. The specific capacitance of both electrodes in difference salt solutions decreased with the following order: $\text{KCl} > \text{NaCl} > \text{CaCl}_2 > \text{MgCl}_2$. This related well to various hydrated sizes and valences.

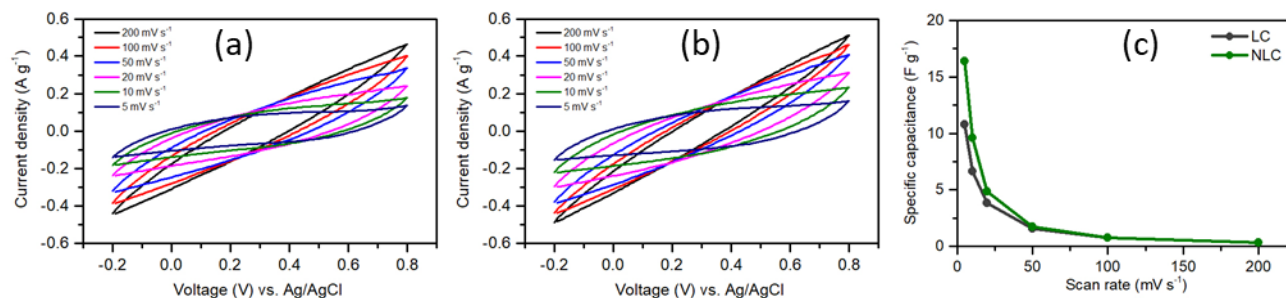


Fig. S6 CV curves of the LC (a) and NLC (b) electrodes in 10 mM NaCl solution with different scan rates and their corresponding specific capacitance at different scan rates (c).

Fig. S6a and b present the CV curves as a function of scan rate of the LC and NLC electrodes in a low concentration of electrolyte. An oval shape was observed for all electrodes and the calculated specific capacitance with a variation of scan rate was plotted in Fig. S6c.

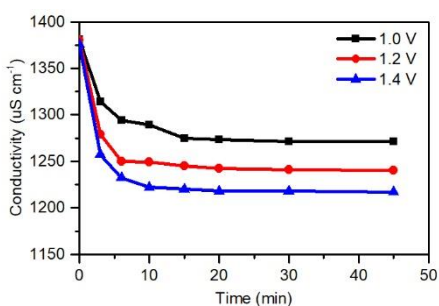


Fig. S7 Effluent conductivity during CDI process with different applied potentials of the NLC electrode in 10 mM NaCl solution.

Effects of operating voltage on the adsorption capacity were studied in the NLC electrode as shown in Fig. S7. The conductivity of solution rapidly dropped in the early stage of the CDI process; subsequently, the conductivity gradually decreased until reaching an equilibrium state. It was found that the change of conductivity increased by increasing applied voltage.

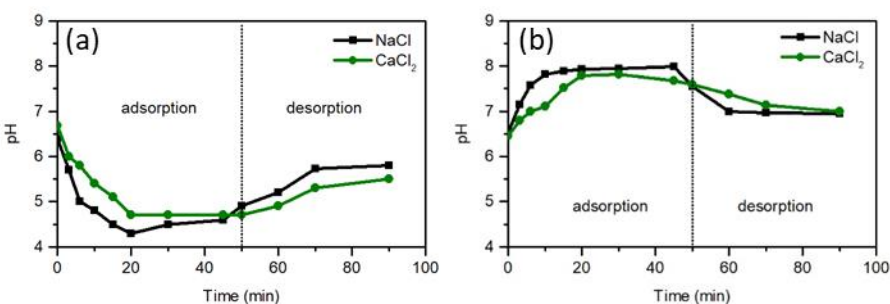


Fig. S8 Effluent pH of the LC (a) and NLC (b) electrodes in 10 mM NaCl and CaCl₂ solution during CDI process.

The effluent pH of the LC electrode was decreased during adsorption step, and subsequently gradually returned to nearly initial value in desorption process, indicating a reversible process (Fig. S8a). Generally, the decreased pH effluent is proposed that carbon oxidation most likely contribute more than Cl⁻ oxidation or water splitting in a limited applied potential.¹⁻⁴ Another reason might be the H⁺ ions exchange which occurs between acidic oxygen-functional group (such as carboxylic groups) on the carbon surface and cations.⁵ Regarding the XPS results, it revealed that LC composed of high oxygen content (9 at%), implying a high amount of oxygen-functional groups (carboxylic or hydroxyl groups) on the carbon surface. Therefore, the results of the LC electrode corresponded to such reasons. In contrast, the NLC electrode exhibited an inverted pH profile. The increase in pH was

observed in the initially adsorption time then almost constant at values between 8. It could be mainly due to a reduction of dissolved oxygen generating hydroxyl ions,^{2,3,5,6} causing a pH increase. However, there was not significantly different pH profile observed between NaCl and CaCl₂ solution.

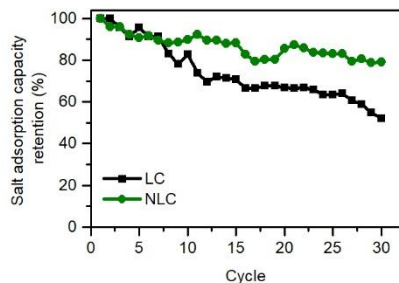


Fig. S9 Cycling stability of the LC and NLC electrodes in 10 mM NaCl solution.

The cycling stability of the LC and NLC electrode was performed in 10 mM NaCl solution for many cycles and the results are shown in Fig. S9. The Γ_{salt} retention (RT_{salt}) is defined to be an index for the cycling stability, which is estimated by equation:

$$R\Gamma_{salt}(\%) = \frac{\Gamma_{salt_n} \times 100}{\Gamma_{salt_i}}$$

where Γ_{salt_n} and Γ_{salt_i} are the salt adsorption capacity at the cycle of n and at the initial cycle, respectively during the cycling stability test.

It was observed that after 30 cycling, the LC electrode remained approximately only 50% retention of salt adsorption capacity while the NLC electrode still remained 80%. This result could suggest that the nitrogen doping improves the stability of the carbon electrode in cycling CDI test.

Table S1 Comparison of electrosorption capacity of various N-doped carbon-based electrode materials.

Sample	SSA (m ² g ⁻¹)	N content (at%)	Initial concentration	Voltage (V)	Electrosorption capacity
<i>N-doped (polymeric based) porous carbon</i>					
N-doped mesostructured carbon nanocrystals (NMCs-800) ⁷	842	6.7	NaCl 584 ppm	1.2	20.63 mg g ⁻¹
N-doped activated carbon (NAC):AC//NAC30 ⁴	1887	2.1	NaCl 8 mM	1.2	24.7 mg g ⁻¹
N-doped highly mesoporous carbon (NOMC) ⁸	459	3.9	NaCl 250 ppm	1.6	26.2 mg g ⁻¹
N-doped hollow carbon sphere (N-PHCS) ⁹	512	2.9	NaCl 500 ppm	1.4	13 mg L ⁻¹
<i>N-doped (bio-based) porous carbon</i>					
N-doped sucrose-derived porous carbon spheres (NPCs-800) ¹⁰	1113	5.8	NaCl 1000 ppm	1.2	14.9 mg g ⁻¹

N-doped pollen- derived porous carbon powder (PC-900) ¹¹	1016	0.71	NaCl 260 ppm	1.4	18 mg g ⁻¹
N-doped cluster-like porous carbons (NCPCs) ¹²	1357	9.2	NaCl 500 ppm	1.6	17.2 mg g ⁻¹
N-doped tamarind fruit shell -derived activated carbon (NTC-800) ¹³	410	n/a	NaCl 600 ppm	1.2	18.8 mg g ⁻¹
Chitosan-based activated carbon (CTS-AC) ¹⁴	2727	13.3	NaCl 500 ppm	1.2	14.1 mg g ⁻¹
Ginklo leaf-derived graphitic N-doped porous carbon ¹⁵	1228	1.7	NaCl 1 M	1.2	16.5 mg g ⁻¹
<i>Monovalent and divalent cation selectivity</i>					
Oxidized-AC and Aminated-AC (O-AC//A-AC) ⁵	1503//1768	n/a	10 mM of NaCl, KCl, MgCl ₂ , CaCl ₂	1.0	Na ⁺ : 0.265, K ⁺ : 0.275, Mg ²⁺ : 0.15, Ca ²⁺ : 0.18 mmol g ⁻¹
Commerical AC ¹⁶	964	-	32 mM of each salt solution	1.0	Na ⁺ : 223, K ⁺ : 237, Mg ²⁺ : 155.3, Ca ²⁺ : 158.8 μmol g ⁻¹
PMMA- <i>b</i> -PAN fibers (PCFs) ¹⁷	640	n/a	NaCl 500, KCl 625, MgCl ₂ : 807, CaCl ₂ : 938 ppm	1.0	Na ⁺ : 0.52, K ⁺ : 0.53, Mg ²⁺ : 0.21, Ca ²⁺ : 0.24 mmol g ⁻¹
Commercial AC ³	540	-	NaCl or KCl 10 mM, CaCl ₂ 5 mM	1.5	NaCl: 0.13, KCl: 0.15, CaCl ₂ : 0.07 mmol g ⁻¹
Porous mordenite modified activated carbon (MOR-AC): MOR-AC//AC ¹⁸	n/a	-	CaCl ₂ 10 mM, mixed salt solution: Ca ²⁺ , Mg ²⁺ , K ⁺ , Na ⁺ ions (2.5 mM each)	1.2	Ca ²⁺ : 248, mixed salt test: Ca ²⁺ : 61, Mg ²⁺ : 57, K ⁺ : 3.6, Na ⁺ : 1.9 μmol g ⁻¹
N-doped lignin-derived porous carbon (NLC) (This work)	645	4.2	10 mM of NaCl, KCl, MgCl ₂ , CaCl ₂	1.2	Na ⁺ : 0.45, K ⁺ : 0.46, Mg ²⁺ : 0.25, Ca ²⁺ : 0.37 mmol g ⁻¹

MCDI: membraned CDI, A-CDI: Asymmetrical CDI, S-CDI: Symmetrical CDI

References:

1. B. Shapira, E. Avraham and D. Aurbach, Side Reactions in Capacitive Deionization (CDI) Processes: The Role of Oxygen Reduction, *Electrochim. Acta*, 2016, 220, 285-295.
2. J. E. Dykstra, K. J. Keesman, P. M. Biesheuvel and A. van der Wal, Theory of pH changes in water desalination by capacitive deionization, *Water Res.*, 2017, 119, 178-186.
3. A. Hassanvand, G. Q. Chen, P. A. Webley and S. E. Kentish, A comparison of multicomponent electrosorption in capacitive deionization and membrane capacitive deionization, *Water Res.*, 2018, 131, 100-109.
4. C.-C. Hsu, Y.-H. Tu, Y.-H. Yang, J.-A. Wang and C.-C. Hu, Improved performance and long-term stability of activated carbon doped with nitrogen for capacitive deionization, *Desalination*, 2020, 481, 114362.
5. Z. Y. Leong and H. Y. Yang, Capacitive Deionization of Divalent Cations for Water Softening Using Functionalized Carbon Electrodes, *ACS Omega*, 2020, 5, 2097-2106.
6. X. Liu, S. Shanbhag, S. Natesakhawat, J. F. Whitacre and M. S. Mauter, Performance Loss of Activated Carbon Electrodes in Capacitive Deionization: Mechanisms and Material Property Predictors, *Environ. Sci. Technol.*, 2020, 54, 15516-15526.
7. X. Xu, A. E. Allah, C. Wang, H. Tan, A. A. Farghali, M. H. Khedr, V. Malgras, T. Yang and Y. Yamauchi, Capacitive deionization using nitrogen-doped mesostructured carbons for highly efficient brackish water desalination, *Chem. Eng. J.*, 2019, 362, 887-896.
8. S. Tian, J. Wu, X. Zhang, K. Ostrikov and Z. Zhang, Capacitive deionization with nitrogen-doped highly ordered mesoporous carbon electrodes, *Chem. Eng. J.*, 2020, 380, 122514.
9. S. Zhao, T. Yan, H. Wang, G. Chen, L. Huang, J. Zhang, L. Shi and D. Zhang, High capacity and high rate capability of nitrogen-doped porous hollow carbon spheres for capacitive deionization, *Appl. Surf. Sci.*, 2016, 369, 460-469.
10. Y. Liu, T. Chen, T. Lu, Z. Sun, D. H. C. Chua and L. Pan, Nitrogen-doped porous carbon spheres for highly efficient capacitive deionization, *Electrochim. Acta*, 2015, 158, 403-409.
11. Q. Liu, X. Li, Y. Wu, M. Qing, G. Tan and D. Xiao, Pine pollen derived porous carbon with efficient capacitive deionization performance, *Electrochim. Acta*, 2019, 298, 360-371.
12. Y. Li, Y. Liu, J. Shen, J. Qi, J. Li, X. Sun, J. Shen, W. Han and L. Wang, Design of nitrogen-doped cluster-like porous carbons with hierarchical hollow nanoarchitecture and their enhanced performance in capacitive deionization, *Desalination*, 2018, 430, 45-55.
13. V. Muthukumaraswamy Rangaraj, A. Achazhiyath Edathil, Y. Y. Kannagara, J.-K. Song, M. Abu Haija and F. Banat, Tamarind shell derived N-doped carbon for capacitive deionization (CDI) studies, *J. Electroanal. Chem.*, 2019, 848, 113307.
14. Q. Wu, D. Liang, X. Ma, S. Lu and Y. Xiang, Chitosan-based activated carbon as economic and efficient sustainable material for capacitive deionization of low salinity water, *RSC Adv.*, 2019, 9, 26676-26684.
15. Z. Xie, X. Shang, K. Xu, J. Yang, B. Hu, P. Nie, W. Jiang and J. Liu, Facile Synthesis of In Situ Graphitic-N Doped Porous Carbon Derived from Ginkgo Leaf for Fast Capacitive Deionization, *J. Electrochem. Soc.*, 2019, 166, E240-E247.
16. C.-H. Hou and C.-Y. Huang, A comparative study of electrosorption selectivity of ions by activated carbon electrodes in capacitive deionization, *Desalination*, 2013, 314, 124-129.
17. T. Liu, J. Serrano, J. Elliott, X. Yang, W. Cathcart, Z. Wang, Z. He and G. Liu, Exceptional capacitive deionization rate and capacity by block copolymer-based porous carbon fibers, *Sci Adv.*, 2020, 6, eaaz0906.
18. P. Nie, B. Hu, X. Shang, Z. Xie, M. Huang and J. Liu, Highly efficient water softening by mordenite modified cathode in asymmetric capacitive deionization, *Sep. Purif. Technol.*, 2020, 250, 117240.